




## Research Article

# Hydrogeochemical Characteristics and Genesis of the Chazi Geothermal Field Area in Tibet

Mingzhong Song <sup>1</sup>, Xujuan Lang <sup>2,3,4,5</sup>, Zhennan Zhong <sup>1</sup>, Fengxin Kang <sup>6</sup>,  
Dawa Nan,<sup>7</sup> Haoting Li,<sup>8</sup> Haowen Yu,<sup>2</sup> Shaoyun Liu,<sup>9</sup> Sihang Han,<sup>2</sup> and Zhao Liu<sup>2,3,4,5</sup>

<sup>1</sup>No. 6 Institute of Geology and Mineral Resources Exploration of Shandong Province, Weihai, Shandong 264209, China

<sup>2</sup>School of Water Resources & Environment, Hebei GEO University, Shijiazhuang 050031, China

<sup>3</sup>Hebei Province Key Laboratory of Sustained Utilization and Development of Water Resources, Shijiazhuang 050031, China

<sup>4</sup>Hebei Province Collaborative Innovation Center for Sustainable Utilization of Water Resources and Optimization of Industrial Structure, Shijiazhuang 050031, China

<sup>5</sup>Hebei Province Key Discipline of Hydrology and Water Resources, Shijiazhuang 050031, China

<sup>6</sup>Shandong Provincial Bureau of Geology & Mineral Resources, Jinan 250013, China

<sup>7</sup>The Geothermal Geological Team of Tibet, Tibet Bureau of Exploration & Development of Geology and Mineral Resources, Lhasa 850032, China

<sup>8</sup>The Second Hydrogeological Geological Exploration Institute of Anhui Geological Survey Bureau, Wuhu 241000, China

<sup>9</sup>Henan Yellow River Hydrology Survey and Design Institute, Zhengzhou 450000, China

Correspondence should be addressed to Xujuan Lang; [langlan77@163.com](mailto:langlan77@163.com)

Received 9 April 2022; Revised 6 July 2022; Accepted 25 August 2022; Published 23 September 2022

Academic Editor: Peng Hou

Copyright © 2022 Mingzhong Song et al. This is an open access article distributed under the Creative Commons Attribution License, which permits unrestricted use, distribution, and reproduction in any medium, provided the original work is properly cited.

The Chazi geothermal field area is located in the large region of Shigatse in southern Tibet. The geothermal resources in this area are abundant, but their exploitation and utilization are low. By studying the water chemistry and isotope characteristics of geochemical fluids in the study area, information on water chemistry, heat storage temperature, recharge source, recharge elevation, and circulation depth was obtained. These results provide a scientific theoretical basis for improving the genetic mechanism of high-temperature geothermal systems in the study area. The type of geothermal fluid hydrochemicals in this area is mainly  $\text{HCO}_3\text{-Na}$ . The isotopic geochemical method was used to determine that the recharge source of geothermal fluids was atmospheric precipitation, and the recharge elevation was 5200–6000 m. The geochemical thermometer, Na–K–Mg equilibrium diagram, and silica-enthalpy mixed model indicated the shallow and deep thermal storage temperatures of approximately 150 and 200°C, respectively, and the average circulation depth of 1163.38 m in the study area. Combined with the fracture structure and magmatic activity characteristics of the southwest Qinghai-Tibet Plateau, the source, storage, cover, and general situation of the area were preliminarily summarised, and the conceptual model of geothermal origin was established. The results can provide a scientific theoretical basis for the mechanism of high-temperature geothermal systems and subsequent drilling and resource development.

## 1. Introduction

Under the current circumstances of energy conservation and emission reduction, a strategic action plan for energy development is vigorous establishment of renewable energy. As a clean, low-carbon, stable, and continuous noncarbon-based energy source, the use of geothermal resources is indispens-

able to achieve the goals of carbon peak and neutrality [1]. Tibet is the most geothermally active region and accounts for nearly a quarter of over 3,000 identified hydrothermally active areas in China [2, 3].

Numerous studies have been conducted in the Yangbajing, Yangyi, and Dagejia geothermal fields. Ji and Ping et al. investigated the hydrochemical characteristics, genesis, and

evolution of the Yangbajing geothermal field [4–6]. Qinghai and Chen studied the chemical anomaly of tungsten present in a high-temperature spring in the Targejia field [7]. Shijuan analysed the source of medium- and high-temperature geothermal fluids in Cuonna [8]. Qinghai et al. studied the hydrochemical characteristics of Yangyi geothermal field by conducting factor analyses [9]. Many scholars have studied the hydrochemical characteristics and genesis mechanism of geothermal fluids in a high-temperature geothermal display area of Tibet [10, 11]. A complete model of the geothermal system in Yangbajing field was established to improve the genetic model of the high-temperature geothermal system in this area. However, studies have shown that the distribution of geothermal water in the geotropic region of Tibet is highly nonuniform, and the geological background and reservoir characteristics of various geothermal areas are different. Therefore, for this area, the genetic model of a high-temperature geothermal system is not suitable, and this model cannot be directly applied to other geothermal display areas [12]. Located in Xigaze of the Tibet Autonomous Region, the Chazi geothermal area is undergoing rapid urbanisation. The geothermal resources of the region are undeveloped, and hot water is largely discharged in the form of springs, which cause serious waste of resources. Studies in this area have focused on plate tectonics [13–15], sedimentary evolution [16–18], geochemistry [19, 20], geological hazards [21, 22], geochronology [23, 24], and deposit geology [25, 26], with few studies focusing on the hydrogeochemical characteristics, evolution of geothermal fluids, models of geothermal genesis, and genetic conceptual models in the geothermal area. Shaoqiang et al. and Haoting et al. have estimated the temperature of geothermal reservoirs in the Chazi geothermal field by using the silica geothermometer and the chalcedony geothermometer, respectively, and concluded that the geothermal fluid is mixed with cold water in this geothermal field, but temperature correction of the thermal storage has not been conducted [27, 28]. In 1975, the Tibetan Plateau Scientific Expedition and Research Team of the Chinese Academy of Sciences conducted a field investigation of geothermal resources in the Xigaze area and recorded basic information, such as physical geography, eruption, and hydrochemical characteristics of exposed hot springs, in the Journal springs in Tibet [29]. In summary, further studies are required as limited literature is available on the Chazi geothermal area.

This study investigated the hydrochemical characteristics, material sources, and characteristics of geothermal reservoirs in the Chazi geothermal area by using hydrogeochemistry, isotope geochemistry, and mixture models [30]. The investigation of the geothermal genetic mechanism of the Chazi geothermal area can contribute to a good conceptual model of the geothermal system, which can provide proof for the rational development and utilization of the geothermal resources in the area.

## 2. Overview of the Study Area

*2.1. Geological Conditions of the Study Area.* In the southwest of the Qinghai-Tibet plateau and the eastern segment of the Alpine-Himalayan structural belt (Figure 1(a)), the Chazi geo-

thermal area is situated along the Gangdese-Tengchong landmass. Its magma arc zone extends westward, eastward, and northward, and its south borders extend on the fore-arc basin by a deep fault [31].

The exposed strata in this area feature volcanic rocks, sedimentary rocks of the Paleogene Linzizong group and the Quaternary strata. From the base to top, the Linzizong group includes Dianzhong, Nianbo, and Pana Formation. Only the Dianzhong Formation ( $E_{1-2}d$ ) and Pana Formation ( $E_2p$ ) appear in the survey area. The Dianzhong Formation ( $E_{1-2}d$ ) is mainly present in Duozebu Mountain, the southwestern corner of the survey area, and is distributed in clusters around ridges with an exposed area of 3.5 km<sup>2</sup>. The lithology comprises neutral-medium acidic volcanic lava with acid volcanoclastic rock, in the form of light grey to off-white massive rhyolite and rhyolite clastic lava, without a rocky bottom in the survey area. The formation is unconformably overlain by Pana Formation, with a thickness of >1000 m. The Pana Formation ( $E_2p$ ) is developed around the periphery of the Dianzhong Formation, with an exposed area of approximately 9 km<sup>2</sup>. The lithology of the Pana Formation comprises dark grey blocky dacite, trachyte andesite, purple-red blocky andesite, and andesitic and porphyroclastic lava, without a rocky peak in the survey area. Eruption is covered by the Dianzhong Formation with angular unconformity, with a thickness of >2400 m [32, 33].

*2.2. Tectonic Conditions of the Study Area.* The fault structure is the major structure of heat control and conductivity in the study area. Fault development is mainly in NE and NW directions. The NW trending tectonic is a normal fault (Figure 1(b)) with water-blocking features. Boiling hot springs are distributed within a few kilometres along the NW fault zone, where large areas of calcifications and calcified mounds exist. The left region of the NE fault is a water-conducting structure, located in the western thermal area. At its intersection with the NW trending fault, the fracture development leads to a crush zone, which provides a satisfactory channel for the storage of deep hot water and migration of underground hot water. The underground hot water is obstructed by the NW fault and the normal fault during migration, resulting in rising springs [34]. With good hydrogeological conditions, the Quaternary pore groundwater is composed of Holocene alluvium, impingement sand, sand gravel, and Holocene marsh deposits and has high water abundance. The Quaternary pore groundwater, rock weathering fractures, and structural phreatic aquifers flow through the geothermal area from the northwest to southeast.

*2.3. Hydrogeology of the Study Area.* In the study, groundwater area can be classified into pore and fissure water available in loose rock and bedrock, respectively, according to the water-bearing medium. In loose rocks, the pore water is mainly distributed in the intermountain valley and piedmont; this water belongs to the quaternary alluvial type and is mainly supplied by atmospheric precipitation and lateral runoff of groundwater in the bedrock mountain area. The runoff conditions of pore water are strictly controlled by the topography, and this water moves from the front of

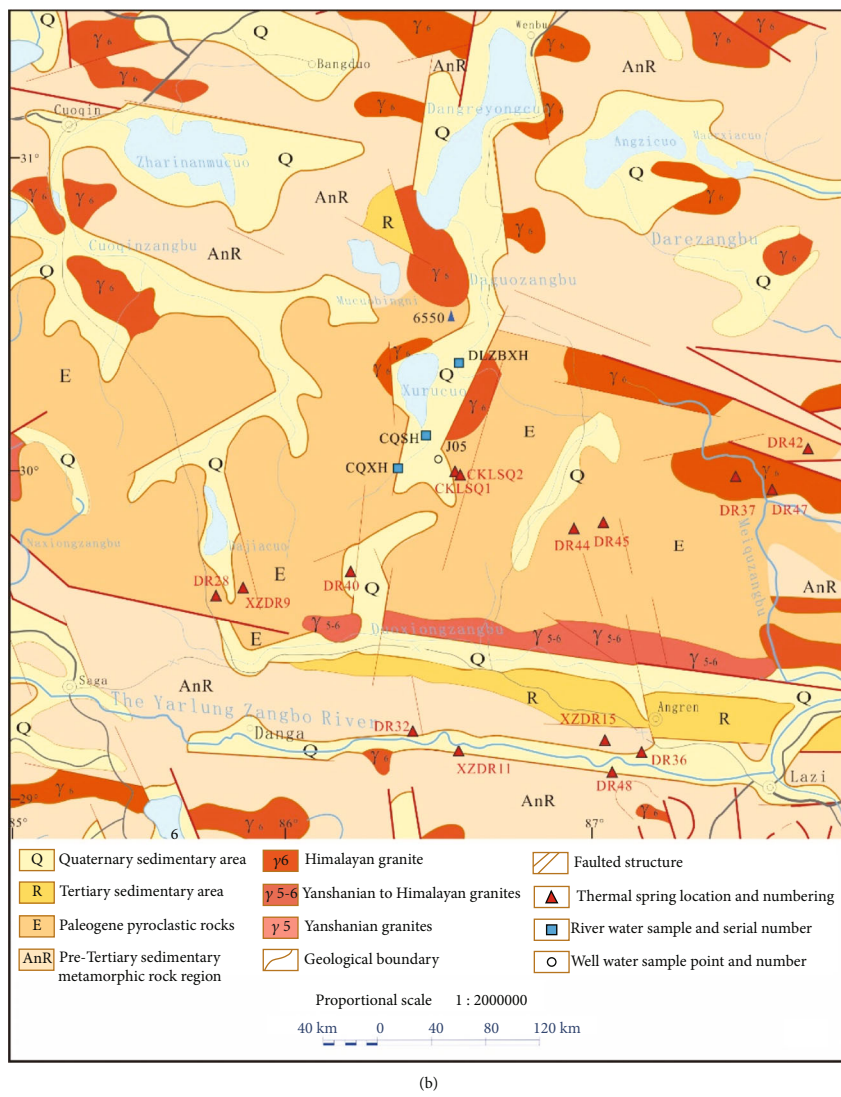
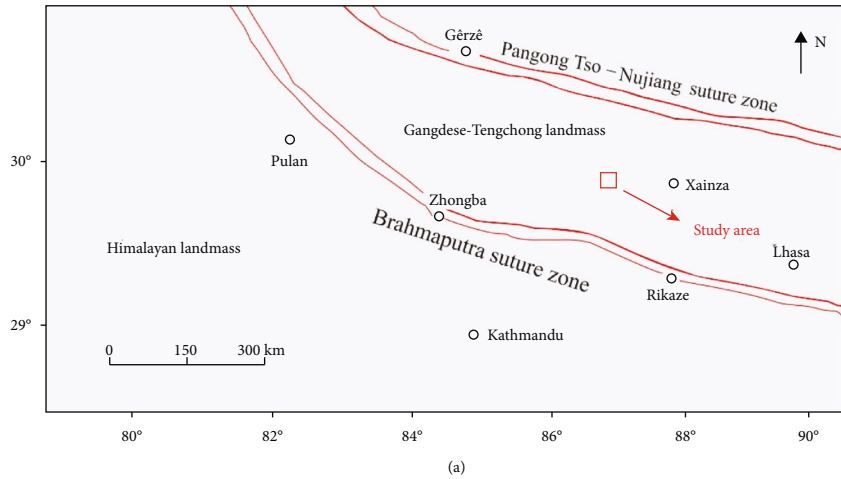


FIGURE 1: Geodetic structure location map and geological sketch of the study area.

the mountain to lowland under the action of gravity. There are two main drainage methods: (1) to supply the water to a river through runoff and (2) to discharge the water in the

form of evaporation. In the bedrock, groundwater is mainly supplied by atmospheric precipitation, and its runoff moves from a high to low ground. This water is drained in the form

TABLE 1: Major constituents of the water samples in the study area.

Field number	Geothermal display area	Sample type	Water temperature/ °C	pH	Na <sup>+</sup>	K <sup>+</sup>	Ca <sup>2+</sup>	Mg <sup>2+</sup>	$\rho_B$ (mg/L)			SO <sub>4</sub> <sup>2-</sup>	TDS	Hydrochemical type
									HCO <sub>3</sub> <sup>-</sup>	CO <sub>3</sub> <sup>2-</sup>	Cl <sup>-</sup>			
DR28	Lagejia spring	Hot spring	85	8.3	386.2	35.1	2.9	0.0	449.2	106.9	158	89.9	1732	HCO <sub>3</sub> -Na
DR32	Semi spring	Hot spring	89	8.7	790.5	125.5	0.7	0.0	571.3	722.8	10.1	4350	4350	Cl·CO <sub>3</sub> -Na
DR36	Charongquren spring	Hot spring	65	7.1	564.7	58.2	53.3	6.7	807.5	0	262.9	436	2333.7	HCO <sub>3</sub> ·SO <sub>4</sub> -Na
DR37	Dengle spring	Hot spring	43	6.6	837.2	72.3	66.8	14.6	1201.1	0	919.3	37.5	3442.1	Cl·HCO <sub>3</sub> -Na
DR40	Pola spring	Hot spring	30	6.6	107.1	5.1	8.5	0.2	99.8	0	90.5	43.6	421.4	Cl·HCO <sub>3</sub> -Na
DR42	Qugu spring	Hot spring	47	8.9	117.9	2.4	0.7	<0.1	268.9	20.9	4.2	12.2	469.2	HCO <sub>3</sub> -Na
DR44	Seluo spring	Hot spring	44	6.7	195.0	40.2	195.8	37.7	1105.2	0	226.6	2.9	1893.1	HCO <sub>3</sub> -cl-ca·Na
DR45	Cha spring	Hot spring	48	7.1	476.4	26.6	70.9	9.2	1246.5	0	200.5	28.3	2242.3	HCO <sub>3</sub> -Na
DR47	Qugulongbu	Hot spring	66	6.9	454.7	25.3	50.3	7.6	616.9	0	280.6	250.8	1903.5	HCO <sub>3</sub> -cl-Na
DR48	Shalei spring	Hot spring	75	7.7	115.4	10.4	28.8	7	378.5	0	7.2	59.2	710.3	HCO <sub>3</sub> -Na
XZDR9	Tamaquzhen	Hot spring	63	7.2	407.4	31.6	40	12.6	856.3	0	190.5	78.2	1919	HCO <sub>3</sub> -Na
XZDR11	Yinjianquzhen	Hot spring	39	6.5	59.4	5.4	210	20.9	811.9	0	8.9	34.8	1113	HCO <sub>3</sub> -Ca
XZDR15	Gabadanni	Hot spring	67	7.0	451.4	29.7	19.2	<0.1	584.4	0	259.4	169.9	1922	HCO <sub>3</sub> -Cl-Na
CKLSQ1	Chazi Village	Hot spring	87	7.8	481.9	39.1	12.8	<0.1	654.9	87.1	165.1	121.9	1806.9	HCO <sub>3</sub> -Na
CKLSQ2	Chazi Village	Hot spring	74	7.9	476.9	41.1	9.5	<0.1	707.3	58.1	167.8	117.5	1844.1	HCO <sub>3</sub> -Na
CQSH	Chazi Village	Chaqu River water	7.5	7.5	13.1	1.4	40.9	6.6	115.9	0	1.41	47.3	279	HCO <sub>3</sub> ·SO <sub>4</sub> -Ca
CQXH	Chazi Village	Chaqu River water	25.5	8.6	363.7	30.1	19.2	1.82	424.1	108.2	118.1	106.1	1386.1	HCO <sub>3</sub> -Na
DLZBXH	Chazi Village	Dalong Zangbo River water	6.5	8.3	8.1	2.5	44.5	4.9	78.4	1.1	3.1	75.3	233.2	SO <sub>4</sub> ·HCO <sub>3</sub> -Ca
J05	Chazi Village	Well water	4	7.5	5.7	2.3	2.5	2.1	78.7	0	2.7	16.6	115.6	HCO <sub>3</sub> -Ca
DR28-1	Lagejia spring	Hot spring	85.5	9.1	365	41	7.2	1.9	261	234	165	132	1570	CO <sub>3</sub> -Cl-HCO <sub>3</sub>
DR28-2	Lagejia spring	Hot spring	78	8.4	388.9	35	0.6	0.2	590.6	36	112.1	102	1712	HCO <sub>3</sub> -Na
DR28-3	Lagejia spring	Hot spring	85	8.7	350	39	0	0	447.2	100.8	151.7	77.8	1600	HCO <sub>3</sub> -Na
DR32-1	Semi spring	Hot spring	86	8.7	700	104	3.4	4.2	490	306	674	65.8	4340	Cl·CO <sub>3</sub> ·HCO <sub>3</sub> -Na
DR42-1	Qugu spring	Hot spring	45	8.9	118	2.5	3.4	1.3	227	45.7	13.9	28.8	227	HCO <sub>3</sub> -CO <sub>3</sub> ·SO <sub>4</sub> -Cl-Na
DR44-1	Seluo spring	Hot spring	40	7.3	175	33.3	202	22.9	1040	—	157	74	1380	HCO <sub>3</sub> -Cl-Ca-Na
DR45-1	Cha spring	Hot spring	44.5	7.3	443	26.5	73.8	12.5	1130	—	172	32.9	1560	HCO <sub>3</sub> -Cl-Na-Ca
DR47-1	Qugulongbu	Hot spring	65.2	7	442.5	26.5	53.2	9.4	493	—	272	280	1600	HCO <sub>3</sub> -Cl-Na-Ca
DR48-1	Shalei spring	Hot spring	76	7.5	125	12.5	34.3	8.3	38.1	—	9.6	26.8	510	HCO <sub>3</sub> -Na-Ca
CKLSQ-1	Chazi Village	Hot spring	87	7.9	468	45	12	4.2	801	—	163	144	1560	HCO <sub>3</sub> -Cl·SO <sub>4</sub> -Na

\*Note: DR28-1, DR28-2, DR28-3, DR32-1, DR42-1, DR44-1, DR45-1, DR47-1, DR48-1, and CKLSQ-1 are quoted from the report of Wei et al. [29].

TABLE 2: Trace components of the water samples in the study area.

Field number	$\rho_B/(mg/L)$										
	HBO <sub>2</sub>	SiO <sub>2</sub>	Fe <sup>2+</sup>	Fe <sup>3+</sup>	F <sup>-</sup>	NO <sub>3</sub> <sup>-</sup>	NO <sub>2</sub> <sup>-</sup>	PO <sub>4</sub> <sup>3-</sup>	Li	Sr	As
DR28	421.6	286.9	<0.05	<0.05	25.8	0.3	<0.0033	0.119	6	0.2	8.6
DR32	2130	536.5	<0.05	<0.05	22.4	<0.05	<0.0033	0.119	33.9	0.2	12.2
DR36	50.7	83.9	<0.03	<0.03	8.7	0.8	<0.001	0.0119	3.6	2.7	0.2
DR37	425.6	87.2	0.1	<0.03	8.6	5.2	<0.001	0.0119	14	2.8	4.9
DR40	20.4	55.1	<0.05	<0.05	3.8	1.5	<0.0033	0.119	0.6	0.2	0.5
DR42	6.2	50.2	<0.03	<0.03	3.2	0.02	<0.001	0.0119	0.2	0.3	0.0006
DR44	181.6	34.6	0.2	<0.03	0.9	0.1	<0.001	0.0119	6.2	1.8	0.0006
DR45	165.1	69.7	<0.03	<0.03	0.3	0.1	<0.001	0.0119	3	3.9	0.0006
DR47	200.3	68.4	0.3	<0.03	6.4	0.1	<0.001	0.0119	2.8	2	6.2
DR48	26.6	76.7	<0.03	<0.03	0.2	0.1	<0.001	0.0119	0.3	1.8	0.0006
XZDR9	360.9	170.8	<0.05	0.19	9.4	0.06	<0.0033	0.0119	4.6	1.2	5.6
XZDR11	7.6	40	<0.05	<0.05	0.7	1.6	<0.0033	0.0119	0.3	2.2	0.0002
XZDR15	416.7	138.3	<0.05	0.39	10.5	<0.05	<0.0033	0.0119	6.6	1.1	6
CKLSQ1	116.3	129.9	<0.03	<0.03	15.5	0.1	<0.001	0.0119	2.2	0.7	0.7
CKLSQ2	120.7	144	<0.03	<0.03	16.9	0.1	<0.001	0.0119	2.2	0.7	0.9
CQSH	0.5	35.1	0.98	<0.03	2.4	0.02	<0.001	0.0119	0.01	0.5	0.0049
CQXH	93.6	104.3	0.26	<0.03	12.5	0.1	<0.001	0.0119	1.6	0.6	0.6
DLZBXH	1.8	15.7	<0.03	<0.03	0.3	0.03	<0.001	0.0119	0.04	0.3	0.0008
J05	0.2	—	—	—	0.3	2.5	<0.001	—	—	—	0.0014
DR28-1	440	22.7	—	—	25	—	—	—	7.3	—	5.4
DR28-2	207.8	87.5	—	—	30.4	—	—	—	5.4	—	—
DR28-3	165.6	120	—	—	27.5	—	—	—	12.3	—	5.5
DR32-1	1750	116.2	—	—	13.3	—	—	—	35	—	30.8
DR42-1	8	36	—	—	4.9	—	—	—	<0.1	—	—
DR44-1	160	32.2	—	—	0.9	—	—	—	4.9	—	—
DR45-1	173	57.8	—	—	0.8	—	—	—	2.8	—	—
DR47-1	187	78.8	—	—	3.6	—	—	—	2.7	—	4
DR48-1	25	74.7	—	—	3.5	—	—	—	0.3	—	—
CKLSQ1-1	170	145	—	—	9.7	—	—	—	2.2	—	0.4

of springs and through evaporation and lateral runoff that supplies the pore groundwater of quaternary loose rocks [35].

### 3. Water Sampling and Tests

In this study, field investigation and systematic sampling were conducted in the study area in 2019, and 15 typical hot spring water samples, 3 river water samples, and 1 cold water well sample were collected. The collected samples are numbered as follows: Taagejia Hot Springs (DR28), Semi Hot Springs (DR32), Charong Qurani Hot Springs (DR36), Dingle Hot Springs (DR37), Polah Hot Springs (DR40), Qugu Hot Springs (DR42), Luo Hot Spring (DR44), Rub Hot Spring (DR45), Qugulongbu Hot Spring (DR47), Shalei Hot Spring (DR48), Tamar Quzhen Hot Spring (DR9), Yinjian Quzhen Hot Spring (DR11), Gabu Nidan Hot Spring (DR15), Chazi Hot Springs (CKLSQ1, CKLSQ2), Chaqu River Water (CQSH, CQXH), Darong Tsangbu River Water (DLZBXH), and Lengshui Well (J05). The sampling position

distribution is shown in Figure 1(b). The hydrochemical data of 10 hot springs in the “Tibet Hot Springs” are as follows: Tagejia Hot Springs (DR28-1, DR28-2, DR28-3), Semi Hot Springs (DR32-1), Qugu Hot Springs (DR42-1), Seluo Hot Spring (DR44-1), Rub Hot Spring (DR45-1), Qugulongbu Hot Spring (DR47-1), Shalei Hot Spring (DR48-1), Chazi Hot Spring (CKLSQ-1), and five sets of hydrogen and oxygen isotope data of the Gejia Hot Springs.

The pH, water temperature, geographical location, and altitude of the region were measured during the study. The samples were collected and stored in PTEF bottles, and the sample bottle and sample plug were rinsed thrice before sampling. The samples were placed in a portable refrigerator. The chemical analysis of the water samples was performed at the Central Laboratory of Tibet Geological Survey Bureau. Hydrogen and oxygen isotopes were detected in the Institute of Hydrogeology and Environmental Geology, CAGS. The pH value was measured using the glass electrode method by using a 3-STARpH meter, and the reading accuracy was  $\leq 0.02$ . TDS was tested by employing the dry-



TABLE 3: Ratios of Na and Cl in the study area.

Field number	Geothermal display area	Sample type	$\rho_B/(mg/L)$		Na <sup>+</sup> /Cl <sup>-</sup>
			Na <sup>+</sup>	Cl <sup>-</sup>	
DR28	Lagejia spring	Hot spring	386.2	158	2.4
DR32	Semi spring	Hot spring	790.5	722.8	1.1
DR36	Charongqurene spring	Hot spring	564.7	262.9	2.1
DR37	Dengle spring	Hot spring	837.2	919.3	0.9
DR40	Pola spring	Hot spring	107.1	90.5	1.2
DR42	Qugu spring	Hot spring	117.9	4.2	28.3
DR44	Seluo spring	Hot spring	195	226.6	0.9
DR45	Cha spring	Hot spring	476.4	200.5	2.4
DR47	Qugulongbu	Hot spring	454.7	280.6	1.6
DR48	Shalei spring	Hot spring	115.4	7.2	16.1
XZDR9	Tamaquzhen	Hot spring	407.4	190.5	2.1
XZDR11	Yinjianquzhen	Hot spring	59.4	8.9	6.7
XZDR15	Gabudanni	Hot spring	451.4	259.4	1.7
CKLSQ1	Chazi Village	Hot spring	481.9	165.1	2.9
CKLSQ2	Chazi Village	Hot spring	476.9	167.8	2.8
CQSH	Chazi Village	Chaqu River water	13.1	1.4	9.3
CQXH	Chazi Village	Chaqu River water	363.7	118.1	3.1
DLZBXH	Chazi Village	Dalong Zangbo River water	8.1	3.1	2.6
J05	Chazi Village	Well water	5.7	2.8	2.1
DR28-1	Lagejia spring	Hot spring	365	165	2.2
DR28-2	Lagejia spring	Hot spring	388.9	112.1	3.5
DR28-3	Lagejia spring	Hot spring	350	151.7	2.3
DR32-1	Semi spring	Hot spring	700	674	1.0
DR42-1	Qugu spring	Hot spring	118	13.9	8.5
DR44-1	Seluo spring	Hot spring	175	157	1.1
DR45-1	Cha spring	Hot spring	443	172	2.6
DR47-1	Qugulongbu	Hot spring	442.5	272	1.6
DR48-1	Shalei spring	Hot spring	125	9.6	13.1
CKLSQ-1	Chazi Village	Hot spring	468	163	2.9

limit value is 1 mg/L), and  $HBO_2$  and  $F^-$  contents were considerably higher than the limit of medically permitted mineral water (minimum limit values are 50 and 2 mg/L, respectively), indicating the physiotherapy value and utilization prospects. For trace elements, As and  $F^-$  concentrations increased slightly, whereas the B concentration decreased because of three reasons: (1) the content of fluoride ions in alkalinity is higher than in acidity as the fluorine complex is easy to be hydrolysed in an alkaline environment; (2) alkaline water is conducive to the dissolution of fluorine-containing minerals [36]; (3) magma and late enrichment lead to an increase in the As content. The hydrochemical composition of the geothermal fluid in the Chazi geothermal area has not changed considerably in recent years.

The hydrochemistry of surface water in CQSH, CQXH, and DLZBXH was  $HCO_3\text{-}SO_4\text{-}Ca$ ,  $HCO_3\text{-}Na$ , and  $SO_4\text{-}HCO_3\text{-}Ca$  (Figure 2), respectively, with the main cations of  $Ca^{2+}$  and  $Na^+$ , main anions of  $SO_4^{2-}$  and  $HCO_3^-$ , and lower TDS than that of hot spring water. Table 1 presents the differences in the hydrochemical composition

between hot and surface water. However, the hydrochemical composition of the water samples collected on the downstream of Chaqu was similar to that of hot water samples, which could explain the downstream water flowing through the hot water area to mix with the geothermal water due to short runoff distance.

#### 4.2. Source of Materials

**4.2.1. Ionic Component.** The  $Na^+/Cl^-$  ratio is considerable higher than 1 (Table 3), indicating strong dissolution and filtration in groundwater [37, 38]. Hot water exhibits strong dissolution for the surrounding rocks during upwelling, enabling  $Na^+$ ,  $K^+$ , and  $Ca^{2+}$  in the potash feldspar and plagioclase to migrate into the hot water [10, 39]. The pH of the geothermal fluid was 7.83–7.93, a range in which the carbonic acid balance favoured  $HCO_3^-$ . The  $HCO_3^-$  content in the fluid samples collected in downstream Chaqu (CQXH) was drastically higher than that in upstream Chaqu presumably because the lateral runoff

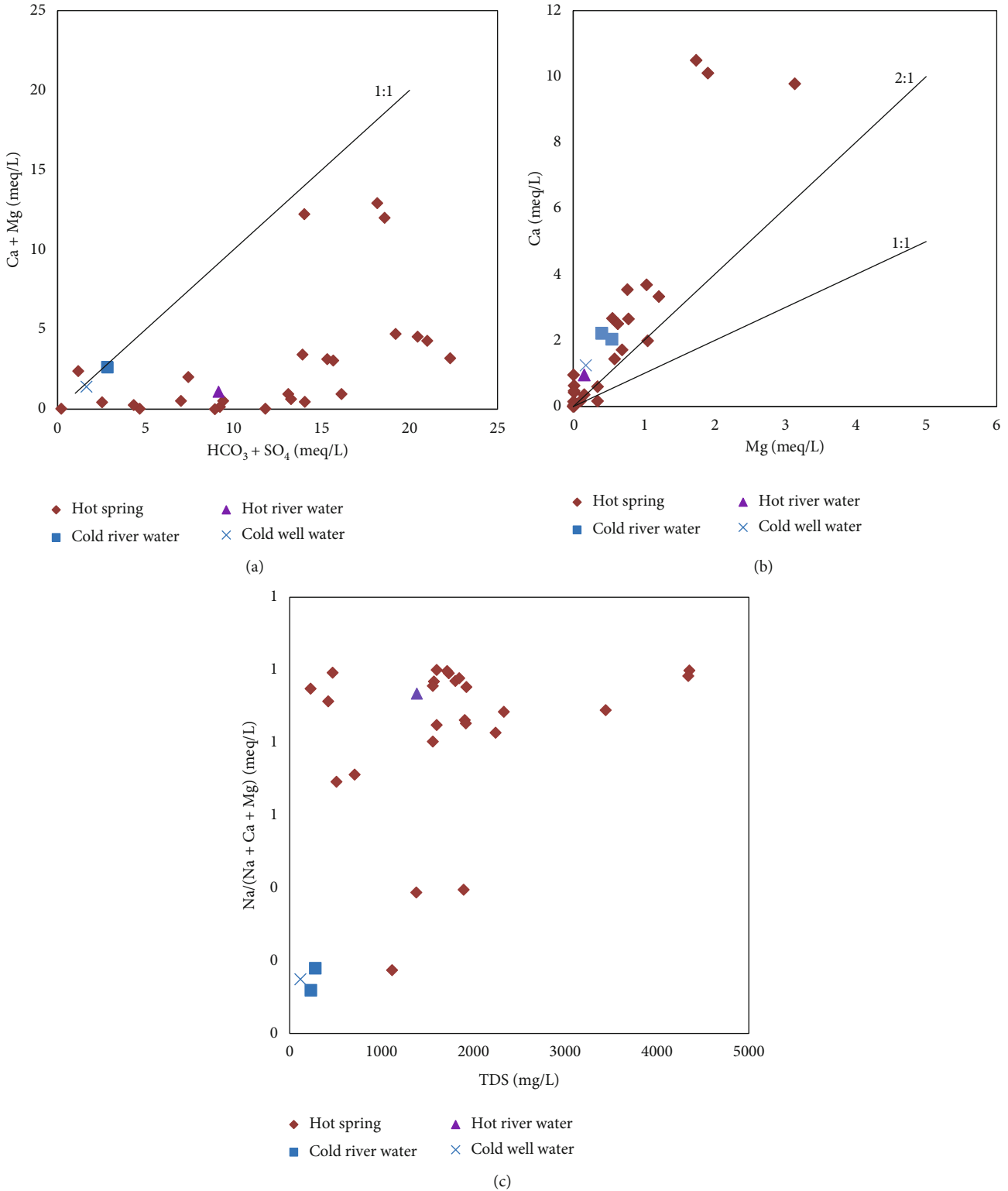


FIGURE 3: Ratio diagrams of the ions of water samples in the study area.

occurred during the vertical upwelling of geothermal water and was subsequently mixed into the river [40].

Almost all the thermal spring samples in the study area are observed below the 1 : 1 line (Figure 3(a)), indicating that considerable ion replacement occurs during runoff. The low concentrations of  $Ca^{2+}$  and  $Mg^{2+}$  (Table 1) suggest that in

the water,  $Ca^{2+}$  and  $Mg^{2+}$  are replaced with absorbed  $Na^+$  in the surrounding rock. The  $\gamma Na/\gamma (Na + Ca + Mg)$  content of hot water is higher than that of cold water, and the value is close to 1 (Figure 3(c)), which indicates considerable ion exchange between  $Na^+ - Ca^{2+}$  and  $Na^+ - Mg^{2+}$  in geothermal fluids in this area.  $Ca^{2+}$  and  $Mg^{2+}$  available in the



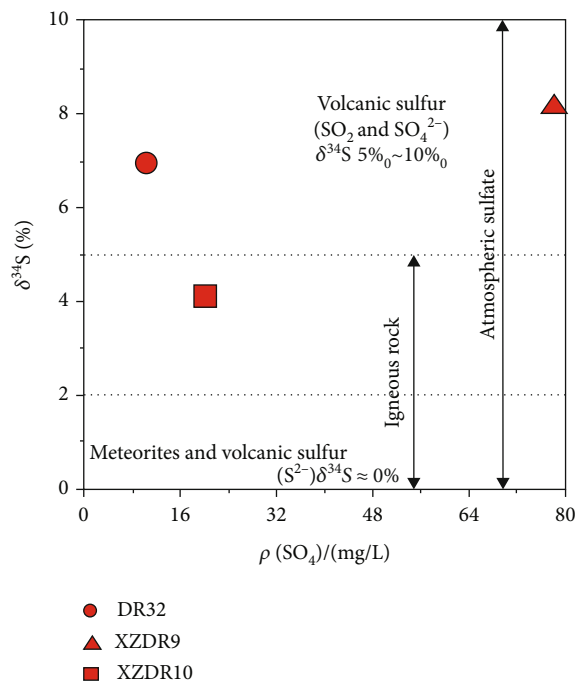


FIGURE 4:  $\delta^{34}\text{S}$ - $\rho\text{SO}_4^{2-}$  plot of geothermal water in the study area.

geothermal fluid are replaced with  $\text{Na}^+$  present on the rock and soil surfaces, which confirmed the aforementioned speculation. Almost all the fluids are distributed above the 2:1 line (Figure 3(b)), which indicates that the main mineral dissolved by carbonate in groundwater is calcite.

The high concentration of  $\text{SO}_4^{2-}$  is a major result of the strong dissolution of geothermal fluids that occurs in the bottom strata of the Paleogene Pana formation ( $E_{2p}$ ) dominated by dacite, andesite, and andesitic and porphyroclastic lava according to the aforementioned discussion [41]. In the study area, the variation range of  $\delta^{34}\text{S}$  is small, and all fall within the range of atmospheric sulphate (Figure 4). The  $\delta^{34}\text{S}$  of DR32 and XZDR9 deviated from the sulphur of meteorites, suggesting that the sulphur of DR32 and XZDR9 is mainly leached from the surrounding rocks of the sedimentary cover. The  $\delta^{34}\text{S}$  of XZDR10 is close to that of meteorite sulphur, indicating that the sulphur source is located deep within the earth's crust and may be regenerated magma produced by remelting in the crust. The mixing of deep sulphur is uniform, and no significant sulphur isotope differentiation can be observed in the geothermal fluid ascent. Some geothermal water samples located in the atmospheric sulphate range are distributed in the volcanic sulphur ( $\text{SO}_2$  and  $\text{SO}_4$ ) range. The geological conditions and the fact that no volcanic activity occurs in the study area indicate that the sulphur in geothermal fluids is caused by the dissolution of the surrounding rocks.

The main sources of  $\text{Cl}^-$  are human activities, deep magma, and leaching effects on rocks. Because this area is vast and not populous, with few  $\text{Cl}^-$  minerals in the stratum, it is speculated that  $\text{Cl}^-$  in geothermal fluids may come from deep magma. The  $\text{Cl}^-$  concentration in the hot springs of the study area is approximately 200mg/L; however, that in the

Semi spring and Dengle spring is higher (Table 1). The deep matter in these two hot springs is speculated to mix to a large extent. The low  $\text{Cl}^-$  content of the Shalei spring distributed near the Yarlung Zangbo River may be caused by mixing with river water.

**4.2.2. Trace Elements.** In general, the  $\text{F}^-$  concentration in the hot water in the study area is high, which is related to the presence of fluorine-containing minerals feldspar and biotite in the strata (Table 2) [42]. Under natural conditions, B and Li in the groundwater majorly originate from the dissolution of related minerals in rocks. The B and Li concentrations in geothermal fluids are positively correlated with the  $\text{Cl}^-$  concentration (Figure 5), indicating that B, Li, and  $\text{Cl}^-$  have the same material source. In addition to the dissolution of rock minerals, other sources are responsible for high B and Li concentrations [43–46]. Studies have revealed that B, Li, Rb, and As in the geothermal water in Tibet originate from the residual magma in the late-stage magmatism [47]. Considering the geothermal and geological conditions of this area, the rich content of Li and Sr in the hot water might be caused by the long-term leaching effect of deep geothermal fluids on volcanic rock formation (Paleogene Dianzhong Formation ( $E_{1-2d}$ )).

### 4.3. Isotope Characteristics of the Geothermal Fluids

**4.3.1. Source of Recharge.** Hydrogen and oxygen isotopes are typically used to trace the recharge source for the groundwater, determine the intensity of groundwater runoff, and identify the water-rock interaction between the groundwater runoff and surrounding rocks [48–50]. Craig analysed the  $\delta^2\text{H}$  and  $\delta^{18}\text{O}$  values of more than 400 natural water samples on a global scale and obtained the global meteoric water line:  $\delta^2\text{H} = 8\delta^{18}\text{O} + 10$  [51]. Scholars have often used the positional relation between the hydrogen and oxygen stable isotope data in the study area to determine the replenishment source of underground fluids [51].

In this study, the hydrogen and oxygen isotope data measured for 6 samples and that collected for 5 samples (Table 4) were used to analyse the recharge source and recharge elevation of the geothermal fluid in the area. Figure 6 reveals that all the hydrogen and oxygen isotopes were distributed near the global atmospheric rainfall equation line [51], indicating that the main recharge source for the underground hot water system was atmospheric rainfall. Moreover, the  $\delta^{18}\text{O}$  and  $\delta^2\text{H}$  of the geothermal fluid and surface water did not differ considerably, which indicated that the recharge source of the underground hot and surface water comes from the surrounding atmospheric precipitation infiltration and not through long-distance migration; that is, the water-rock interaction is not strong [52, 53]. Another possible reason is that the geothermal fluids in the study area were mixed with surface cold water during the rising process.

**4.3.2. Recharge Elevation.** The  $\delta^2\text{H}$  and  $\delta^{18}\text{O}$  of atmospheric precipitation often exhibit the characteristics of temperature, continental, seasonal fluctuation, etc. The following method can be used to estimate the replenishment elevation

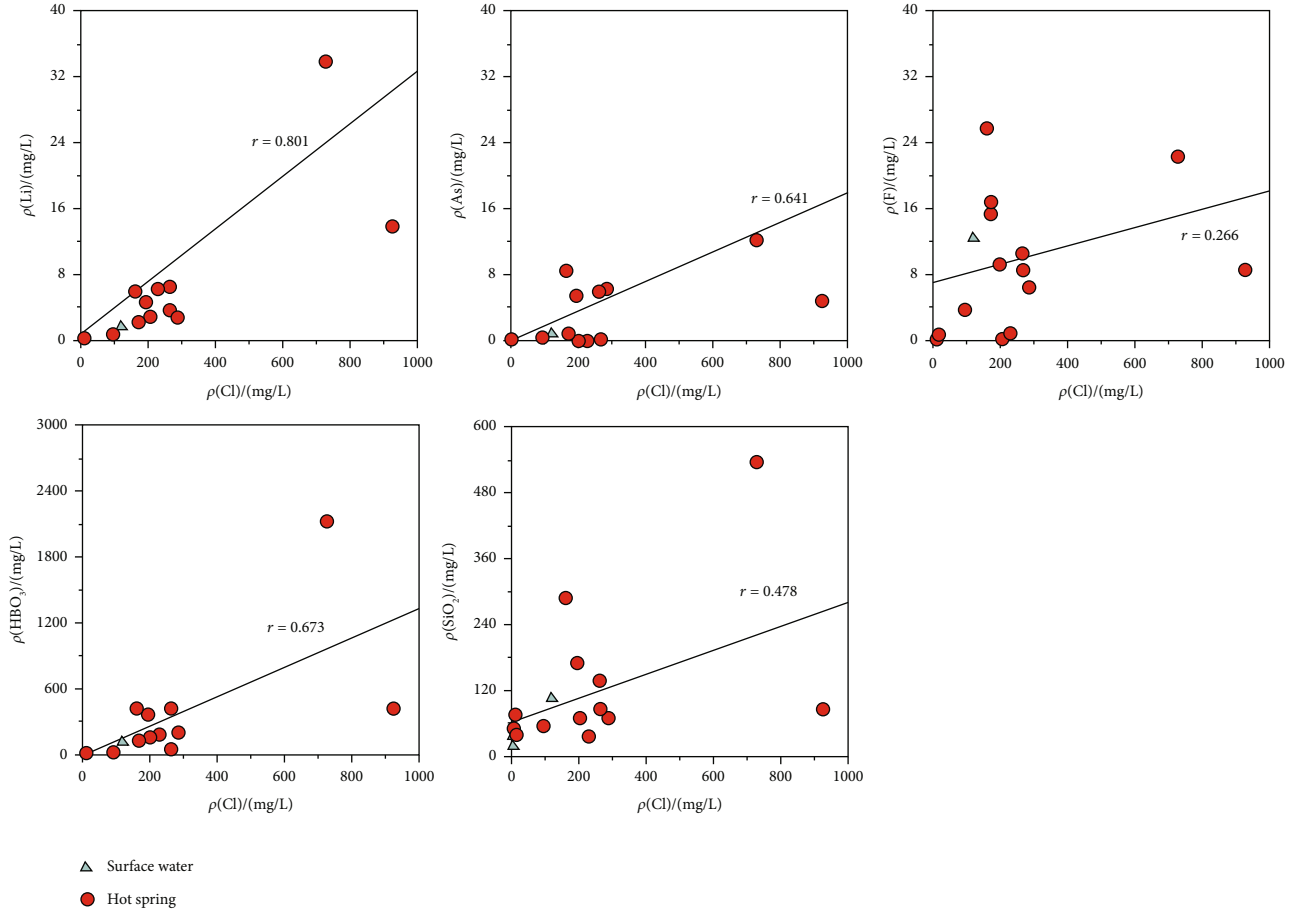


FIGURE 5: Correlation diagram between trace components and  $\text{Cl}^-$  in the study area.

TABLE 4: Data of  $\delta^2\text{H}-\delta^{18}\text{O}$  of the geothermal fluid in the study area.

Field number	Geothermal display area	Sample type	$\delta^2\text{H}_{\text{VSMOW}}(\text{‰})$	$\delta^{18}\text{O}_{\text{VSMOW}}(\text{‰})$	Data sources
DR28-1	Lagejia spring	Hot spring	-149	-18.6	Quoted from literature [47]
DR28-2	Lagejia spring	Hot spring	-154	-18.6	
DR28-3	Lagejia spring	Hot spring	-153	-18.6	
DR28-4	Xiaolupang spring	Hot spring	-155	-18.6	
CMQ	Changmaqu River water	River water	-130	-18.3	Measured
CKLSQ1	Chazi Village	Hot spring	-163	-20.5	
CKLSQ2	Chazi Village	Hot spring	-163	-20.6	
CQSH	Chazi Village	River water	-136	-17.6	
CQXH	Chazi Village	River water	-148	-18.7	
DLZBXH	Chazi Village	River water	-164	-20.9	

of each hot spring in the study area based on the elevation effect of the stable isotope of oxygen.

$$H = \frac{\delta_G - \delta_P}{K} + h, \quad (1)$$

where  $H$  is the recharge elevation, m;  $h$  is the elevation of the sampling point, m;  $\delta_G$  is the  $\delta^{18}\text{O}$  of the hot spring, ‰;  $\delta_P$  is the  $\delta^{18}\text{O}$  of the atmospheric precipitation, ‰;  $K$  is the eleva-

tion gradient of the  $\delta^{18}\text{O}$  of the atmospheric precipitation,  $\delta/100\text{ m}$ . In this paper, the CQSH data ( $\delta^{18}\text{O}$  is  $-17.6\text{‰}$ ) at the upstream point of Chaqu is used as the  $\delta^{18}\text{O}$  value of atmospheric precipitation in Chazi Hot Spring, and the CMQ ( $\delta^{18}\text{O}$  is  $-18.29\text{‰}$ ) at the Changmaqu River water point is used as the  $\delta^{18}\text{O}$  value of atmospheric precipitation in the Gejia Hot Spring. The elevation gradient of  $\delta^{18}\text{O}$  in Tibet ( $-0.26\text{‰}/100\text{ m}$ ) is used as the  $K$  value [54]. The calculation results are presented in Table 5.

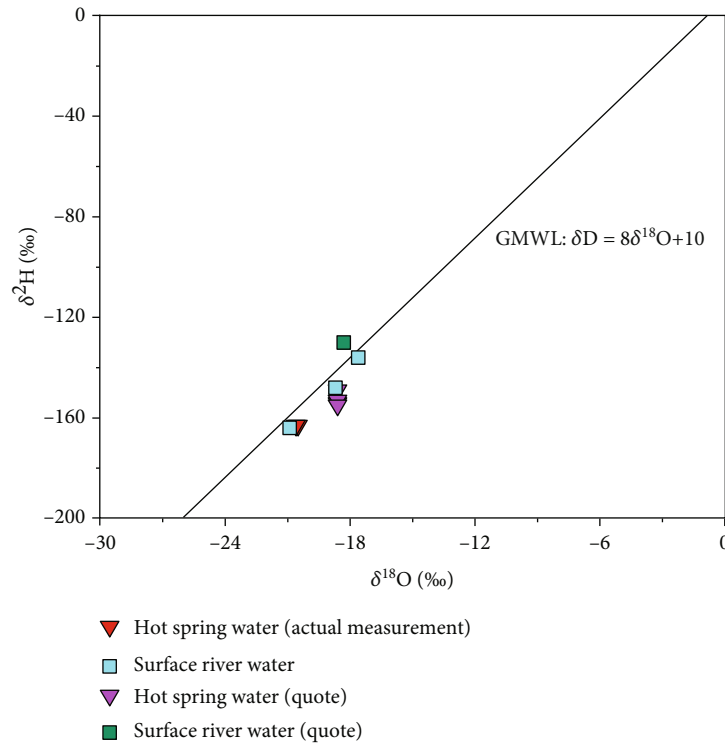


FIGURE 6:  $\delta^2\text{H}-\delta^{18}\text{O}$  isotope relationship of various water samples.

TABLE 5: Calculated values of the geothermal fluid replenishment elevation in the study area.

Field number	CKLSQ1	CKLSQ2	DR28-1	DR28-2	DR28-3	DR28-4
Sampling elevation	4841	4837	5054	5058	5047	5050
Replenishment elevation	5956	5990	5165	5188	5177	5184

TABLE 6: Geothermometer function of geothermal water in the study area.

Geothermometers	Calculation formula	Scope of application
Quartz1	$T = \frac{1309}{5.19 - \log \text{SiO}_2} - 273.15$	No loss of steam
Quartz2	$T = \frac{1522}{5.75 - \log \text{SiO}_2} - 273.15$	Maximum steam loss 0-250°C
Chalcedony1	$T = \frac{1032}{4.69 - \log \text{SiO}_2} - 273.15$	High temperature thermal storage
Chalcedony2	$T = \frac{1264}{5.31 - \log \text{SiO}_2} - 273.15$	Maximum steam loss
Na-K	$T = \frac{1217}{\log (\text{Na/K}) + 1.483} - 273.15$	$t > 150^\circ\text{C}$

The geothermal fluid replenishment elevation range of the study area is 5200–6000 m (Table 5). This estimated value is close to the elevation data of the sampling point. It is inferred that the replenishment of geothermal water mainly comes from atmospheric rainfall infiltration replenishment received by the mountains near the hot spring outcrop area and a small amount of alpine snowmelt replenishment.

#### 4.4. Temperature of Geothermal Reservoirs and Cycle Depth Estimation

4.4.1. Geochemical Geothermometer for the Temperature Estimation of Geothermal Reservoirs. The geothermometer is an effective method for estimating the temperature of thermal storage, and each temperature scale has certain

TABLE 7: Estimated results of the reservoir temperature in the study area.

Field number	Sampling temperature/ $^{\circ}\text{C}$	$\text{SiO}_2$ geoth				Cation geoth Na-K/ $^{\circ}\text{C}$
		Quartz geoth (minimum steam loss)/ $^{\circ}\text{C}$	Quartz geoth (maximum steam loss)/ $^{\circ}\text{C}$	Chalcedony geoth (minimum steam loss)/ $^{\circ}\text{C}$	Chalcedony geoth (maximum steam loss)/ $^{\circ}\text{C}$	
DR28	85	—	189.2	—	170	224.8
DR32	89	—	230.8	—	216.7	251.8
DR36	65	127.6	—	99.9	—	234.7
DR37	43	129.7	—	102.1	—	220.8
DR40	30	106.4	—	76.8	—	179.8
DR42	47	102	—	72.1	—	131.6
DR44	44	85.4	—	54.4	—	297.4
DR45	48	117.9	—	89.3	—	189.6
DR47	66	117	—	88.3	—	189.3
DR48	75	122.9	—	94.7	—	223.9
XZDR9	63	169.4	—	146.8	—	212.7
XZDR11	39	91.7	—	61.1	—	224.9
XZDR15	67	156.2	—	131.7	—	201
CKLSQ1	87	—	145.4	—	122.3	216.2
CKLSQ2	74	158.7	—	134.5	—	220.6

assumptions. Therefore, when using the geothermometers to study the temperature of the thermal reservoir, the applicable scope and conditions of each temperature scale should be considered to select a suitable geothermometer to estimate the thermal storage temperature. The commonly used geothermometers mainly include cationic geochemistry,  $\text{SiO}_2$  geothermometer, isotope geothermometer, and gas geothermometer, among which the most commonly used are cationic geochemistry and  $\text{SiO}_2$  geothermometers. According to the hydrochemical characteristics of the geothermal fluid in the study area, the geothermal geology, and the applicable conditions of the geothermal geothermometers (Table 6), this study used the  $\text{SiO}_2$  geothermometer (quartz, chalcedony) and Na-K geothermometer to estimate thermal storage temperature for the study area [55–57]. Because the study region is located in a high-altitude area in Tibet, the boiling point of water is low. In this study, we designated the hot springs with exposure temperatures of  $>80^{\circ}\text{C}$  as boiling springs. That is, when the exposure temperature of the sampling point was  $\geq 80^{\circ}\text{C}$ , the maximum steam loss formula was used when the  $\text{SiO}_2$  geothermometer was used to estimate thermal storage temperature. When the exposure temperature of the sampling point did not reach  $80^{\circ}\text{C}$ , the no-steam loss formula was used. The calculation results are shown in Table 7.

The reservoir temperature calculated using chalcedony (minimum steam loss) is not the true reflection of the hydrothermal system because the estimated values are not substantially different from the reservoir temperature of the thermal springs (Table 7). The reservoir temperatures estimated using quartz and chalcedony geothermometer (maximum steam loss) of DR28, DR32, and CKLSQ1 are the same, indicating that the temperatures acquired using this formula are highly reliable (Table 7). For other sample

points, the reservoir temperature calculated using quartz geothermometer (no steam loss) is mostly distributed in  $120\text{--}160^{\circ}\text{C}$ , with an average of  $126^{\circ}\text{C}$ . The estimated values are slightly low combined with the geothermal background. The estimated value of Na-K geothermometer is higher than that of  $\text{SiO}_2$  geothermometer. The low value of  $\text{SiO}_2$  geothermometer may be caused by the following reasons: (1) the hot spring fluid was mixed with varying degrees of cold water during the ascent. (2) Saturated  $\text{SiO}_2$  dissolved in hot water above  $180^{\circ}\text{C}$  precipitated [48]. From the Na-K-Mg triangle diagram (Figure 7), the groundwater in the study area had not reached a water-rock equilibrium state, and cold water was mixed in the geothermal fluid. This is the probable reason for the low reservoir temperature estimation by using  $\text{SiO}_2$  geothermometer. Most thermal springs are located near the partial equilibrium zone, which shows that the method of reservoir temperature estimation by using the Na-K geothermometer presents certain reference significance. The estimation results acquired using the Na-K geothermometer are considered to reflect deep reservoir characteristics, and those obtained by employing  $\text{SiO}_2$  geothermometer are considered to reflect shallow reservoir characteristics combined with the applicable conditions of Na-K geothermometer.

*4.4.2. Silica-Enthalpy Mixing Model to Estimate the Temperature of Geothermal Reservoirs.* According to the aforementioned analysis, the hot water in the study area is likely to mix with the shallow cold water during the ascent. A strong linear relationship exists between Cl and B in the geothermal fluids (Figure 8). CQSH is the upstream sample, and CQXH is the downstream sample. Most geothermal fluid samples are located at the cold water

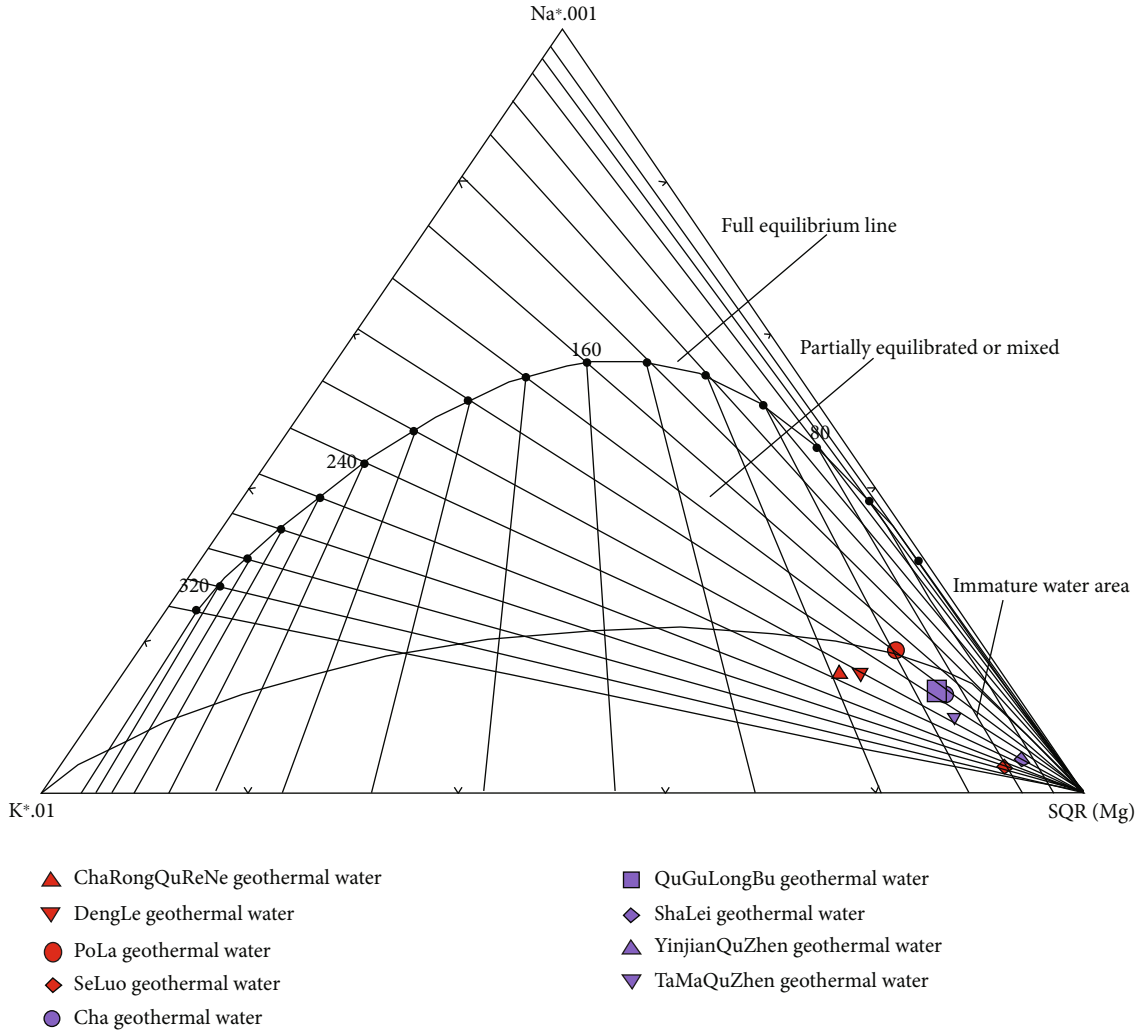


FIGURE 7: Na-K-Mg triangle diagram of the geothermal fluid in the study area.

end (Figure 8). No significant differences can be observed in the compositions of  $\delta^2\text{H}$  and  $\delta^{18}\text{O}$  of the geothermal fluids (Figure 6). Therefore, the geothermal fluid in this area can be considered a mixture of deep geothermal fluids and cold water [58, 59].

In 1974, Fournier and Truesdell developed a silica-enthalpy equation method to estimate the true thermal storage temperature before the cold water is mixed. The principle of this method is that the mixing of hot and cold water inevitably causes the initial enthalpy and  $\text{SiO}_2$  content of deep water to decrease to the final enthalpy and  $\text{SiO}_2$  content of spring water. According to this principle, the model equation is derived:

$$S_c X_1 + S_h (1 - X_1) = S_s, \quad (2)$$

$$\rho c_{\text{Silica}} X_2 + \rho h_{\text{Silica}} X_2 (1 - X_2) = \rho s_{\text{Silica}}, \quad (3)$$

where  $S_c$  is the enthalpy of cold water (J/g);  $S_s$  is the final enthalpy of spring water (J/g), below  $100^\circ\text{C}$ , and the

enthalpy of saturated water is equal to the water Celsius degree. For  $>100^\circ\text{C}$ , the relationship between temperature and enthalpy of saturated water is presented in Table 8.  $S_h$  is the initial enthalpy of hot water (J/g);  $\rho c_{\text{Silica}}$  is the silica mass concentration of cold water (mg/L);  $\rho s_{\text{Silica}}$  is the silica mass concentration of the spring water (mg/L);  $\rho h_{\text{Silica}}$  is the initial silica mass concentration of hot water (mg/L); and  $X$  is the mixing proportion of cold water.

In this study, the enthalpy of cold water was determined to be the average temperature of the study area at  $5^\circ\text{C}$  in the year, and the final enthalpy of the hot spring was the enthalpy value corresponding to the measured temperature value. The silica mass concentration of cold water (upstream of Chaqu) was  $35.05 \text{ mg/L}$ , and the mass concentration of  $\text{SiO}_2$  in the hot spring takes the actual measured value this time (Table 2). Substitute the concentration into the model equation to obtain the values of  $X_1$  and  $X_2$  for each hot spring point (Table 9), and then, project the calculated values of  $X_1$  and  $X_2$  and their corresponding temperatures into the scatter diagram, two

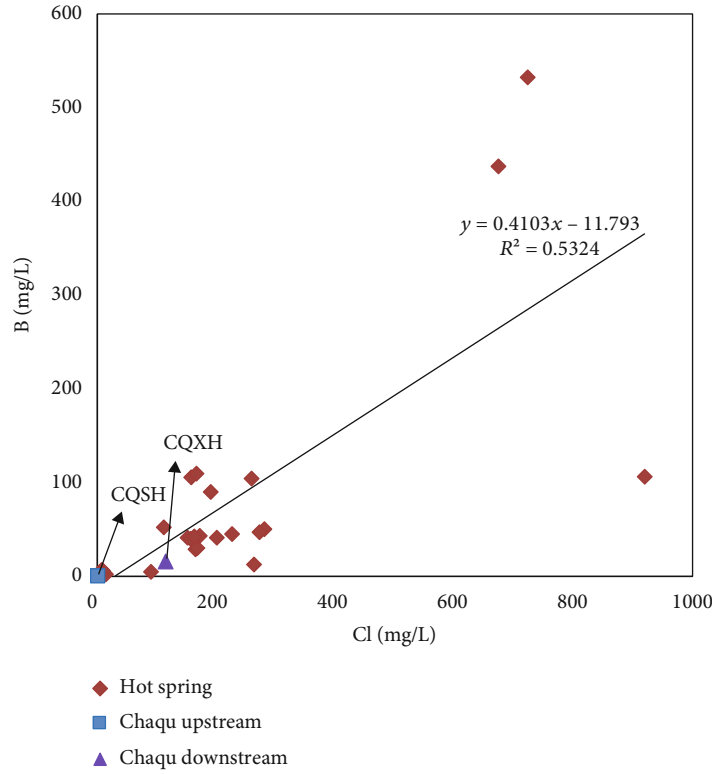


FIGURE 8: Relationship between Cl and B contents in the study area.

TABLE 8: Relationship between water temperature, enthalpy, and mass concentration of  $\text{SiO}_2$ .

$t/^\circ\text{C}$	enthalPy (* 4.1868J/g)	$\rho c_{\text{SiO}_2}/(\text{mg/L})$
50	50	13.5
75	75	26.6
100	100.1	48
125	125.1	80
150	151	125
175	177	185
200	203.6	265
225	230.9	365
250	259.2	486
275	289	614
300	321	692

curves can be drawn. The abscissa corresponding to the intersection of the two curves is the estimated value of heat storage temperature before mixing, and the ordinate corresponding to the intersection of the two curves is the mixing ratio of cold water (Figure 9).

The mixing ratio of cold water in the hot springs in the study area is relatively large, and the heat storage temperature before the cold water mixed is generally above  $150^\circ\text{C}$ , which indicates the characteristics of high-temperature heat storage in the study area (Figure 9). The abnormalities are the five hot springs: DR28, DR32, DR42, DR44, and XZDR9. They present no intersection in Figure 5, indicating that

these five hot springs are affected by the absence of cold water mixing. The thermal storage temperatures of DR36, DR37, DR40, DR45, DR47, DR48, XZDR11, XZDR15, CKLSQ1, and CKLSQ2 before the mixing of cold water are  $170^\circ\text{C}$ ,  $217^\circ\text{C}$ ,  $169^\circ\text{C}$ ,  $169^\circ\text{C}$ ,  $145^\circ\text{C}$ ,  $149^\circ\text{C}$ ,  $104^\circ\text{C}$ ,  $241^\circ\text{C}$ ,  $200^\circ\text{C}$ , and  $234^\circ\text{C}$ , respectively, and their mixing ratios of cold water are 64%, 82%, 85%, 74%, 57%, 52%, 65%, 74%, 59%, and 71%, respectively.

In summary, the average mixing ratio of hot spring and cold water in the study area is 75%, and the average value of the heat storage temperature before the cold water mixed is  $200^\circ\text{C}$ , which is basically the same as the heat storage temperature obtained in the Na-K-Mg balance diagram and the result of the Na-K geothermometer. This reflects the real storage temperature before the cold water is mixed in the study area, that is, the deep heat is stored in the study area. The calculation results of the  $\text{SiO}_2$  (maximum steam loss) geothermometer are distributed around  $150^\circ\text{C}$ , indicating shallow heat storage in the study area.

**4.4.3. Circulation Depth.** The foregoing hydrogen and oxygen isotope research results showed that the geothermal fluid in the study area is mainly of atmospheric rainfall replenishment, and the temperature of hot water chiefly depends on deep-circulation geothermal heating. Therefore, the calculation of the temperature of underground hot water storage can be used to estimate the cycle depth of the hot water with the following formula:

$$Z = G(T_z - T_0) + Z_0, \quad (4)$$

TABLE 9: Calculated values of  $X_1$  and  $X_2$  hot springs in the study area.

Temperature/ $^{\circ}$ C		50	75	100	125	150	175	200	225	250	275	300
DR28	$X_1$	-0.78	-0.14	0.16	0.33	0.45	0.53	0.6	0.65	0.69	0.72	0.75
	$X_2$	12.69	30.81	-18.45	-4.6	-1.8	-0.68	-0.1	0.24	0.44	0.56	0.62
DR32	$X_1$	-0.87	-0.2	0.12	0.3	0.42	0.51	0.58	0.63	0.67	0.7	0.73
	$X_2$	24.27	60.35	-37.73	-10.16	-4.58	-2.34	-1.18	-0.52	-0.11	0.13	0.24
DR36	$X_1$	-0.33	0.14	0.37	0.5	0.59	0.65	0.7	0.73	0.76	0.79	0.81
	$X_2$	3.27	6.78	-2.77	-0.09	0.46	0.67	0.79	0.85	0.89	0.92	0.93
DR37	$X_1$	0.16	0.46	0.6	0.68	0.74	0.78	0.81	0.83	0.85	0.87	0.88
	$X_2$	3.42	7.17	-3.02	-0.16	0.42	0.65	0.77	0.84	0.88	0.91	0.92
DR40	$X_1$	0.44	0.64	0.74	0.79	0.83	0.85	0.87	0.89	0.9	0.91	0.92
	$X_2$	1.93	3.37	-0.54	0.56	0.78	0.87	0.91	0.94	0.96	0.97	0.97
DR42	$X_1$	0.07	0.4	0.56	0.65	0.71	0.76	0.79	0.81	0.83	0.85	0.87
	$X_2$	1.7	2.79	-0.17	0.66	0.83	0.9	0.93	0.95	0.97	0.97	0.98
DR44	$X_1$	0.13	0.44	0.59	0.68	0.73	0.77	0.8	0.83	0.85	0.86	0.88
	$X_2$	0.98	0.95	1.03	1.01	1	1	1	1	1	1	1
DR45	$X_1$	0.04	0.39	0.55	0.64	0.71	0.75	0.78	0.81	0.83	0.85	0.86
	$X_2$	2.61	5.1	-1.67	0.23	0.62	0.77	0.85	0.9	0.92	0.94	0.95
DR47	$X_1$	-0.36	0.13	0.36	0.49	0.58	0.65	0.69	0.73	0.76	0.79	0.81
	$X_2$	2.55	4.95	-1.58	0.26	0.63	0.78	0.85	0.9	0.93	0.94	0.95
DR48	$X_1$	-0.56	0	0.26	0.42	0.52	0.59	0.65	0.69	0.72	0.75	0.78
	$X_2$	2.93	5.93	-2.22	0.07	0.54	0.72	0.82	0.87	0.91	0.93	0.94
XZDR9	$X_1$	-0.29	0.17	0.39	0.52	0.6	0.66	0.71	0.74	0.77	0.8	0.82
	$X_2$	7.3	17.06	-9.48	-2.02	-0.51	0.09	0.41	0.59	0.7	0.77	0.79
XZDR11	$X_1$	0.24	0.51	0.64	0.72	0.77	0.8	0.83	0.85	0.87	0.88	0.89
	$X_2$	1.23	1.59	0.62	0.89	0.94	0.97	0.98	0.98	0.99	0.99	0.99
XZDR15	$X_1$	-0.38	0.11	0.35	0.48	0.58	0.64	0.69	0.73	0.76	0.78	0.8
	$X_2$	5.79	13.22	-6.97	-1.3	-0.15	0.31	0.55	0.69	0.77	0.82	0.84
CKLSQ1	$X_1$	-0.82	-0.17	0.14	0.32	0.44	0.52	0.59	0.64	0.68	0.71	0.74
	$X_2$	5.4	12.22	-6.32	-1.11	-0.05	0.37	0.59	0.71	0.79	0.84	0.86
CKLSQ2	$X_1$	-0.53	0.01	0.27	0.43	0.53	0.6	0.65	0.69	0.73	0.76	0.78
	$X_2$	6.06	13.9	-7.42	-1.42	-0.21	0.27	0.53	0.67	0.76	0.81	0.83

where  $Z$  is the calculated cycle depth, m;  $G$  is the geothermal heating gradient,  $m/^{\circ}$ C, with a value of  $6.67 m/^{\circ}$ C [60];  $T_z$  is the heat storage temperature,  $^{\circ}$ C, taking the heat storage temperature determined using an existing mixed model;  $T_0$  is the multiyear average temperature of the replenishment area,  $^{\circ}$ C, its value is  $5^{\circ}$ C; and  $Z_0$  is the depth of the normal temperature zone, m, the value is 20 m. The calculation results of the cycle depth are shown in Table 10.

The circulation depths of DR42, DR47, DR48, and XZDR11 hot springs are shallow, ranging from 667 to 974 m (Table 10). The circulation depths of all the other

hot springs are  $>1000$  m. DR32 and XZDR15 hot springs show the maximum circulation depth of 1500 m. Overall, the average circulation depth of the study area is 1163.38 m, and the geothermal conditions are satisfactory.

### 5. Conceptual Model of the Heat Reservoir in the Research Area

5.1. Heat Source in the Study Area. Geophysical surveys showed AMT measurement anomalies, gravity anomalies, and magnetic anomalies present in the study area. The

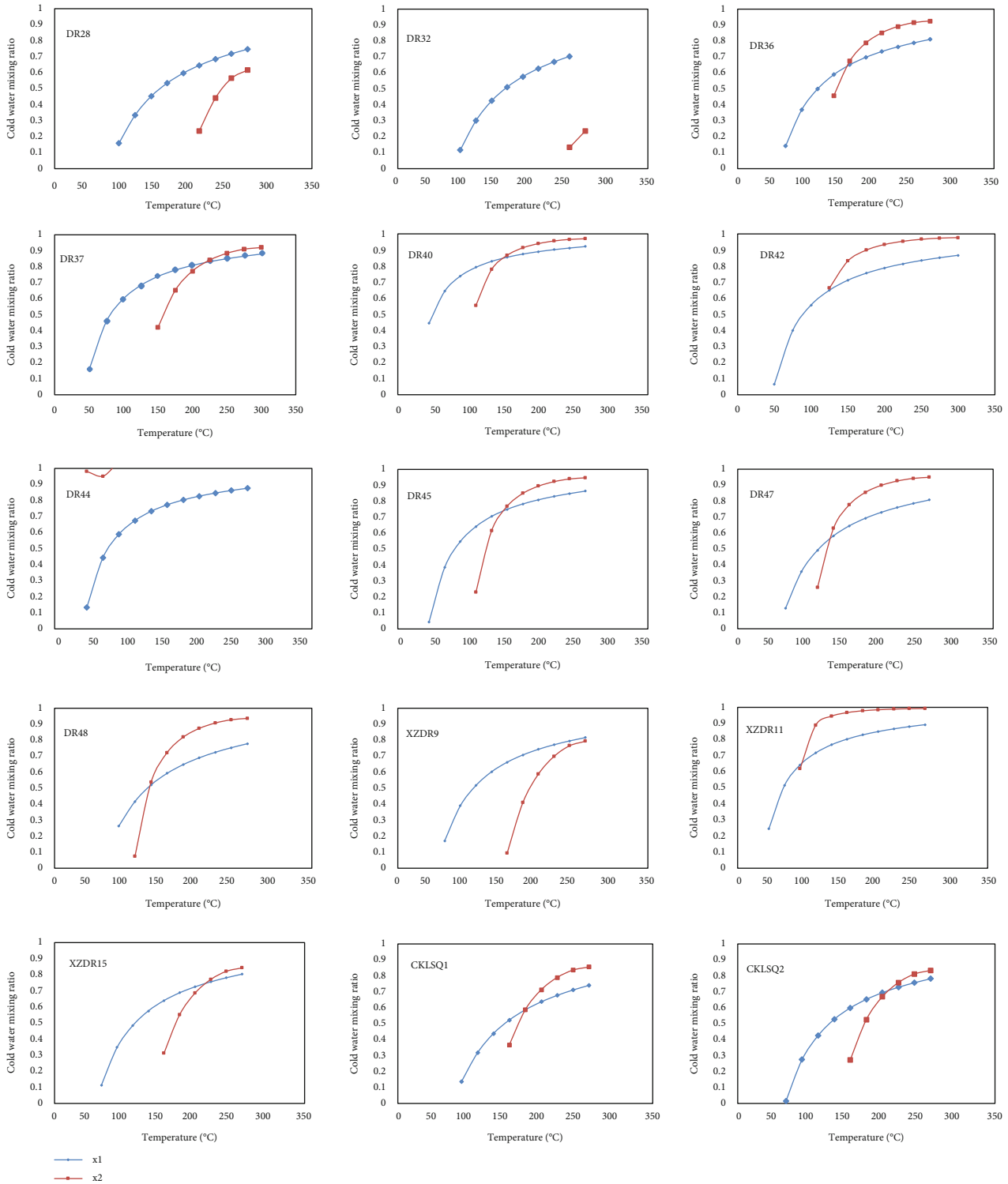


FIGURE 9: Si-enthalpy model of the study area.

gravity field in the area is high and low in the south and north, respectively. The overall appearance is low gravity anomalies, and high gravity anomalies are in some areas. The magnetic anomalies are generally distributed in NE-SW orientation. The Cenozoic, neotectonic activities, mainly composed of active faults, fault basins (fault-sag belts), fault-

block mountains (uplift belts), and accompanying hydrothermal phenomena (hot springs), and seismic activities, are considerably frequent in the study area. Most faults are NW-trending faults dominated by normal and translational faults. The area is mainly the Ranyongcuo-Xurucu fault zone; the faults in the area are mainly distributed in the



TABLE 10: Calculation of underground hot water circulation depth in in the study area.

Field number	Sampling point elevation/m	Reservoir temperature/°C	Cycle depth/m
DR28	5054	202.1	1335
DR32	4262	237.7	1572
DR36	4886	170	1121
DR37	5259	212	1401
DR40	4923	160	1054
DR42	4382	109.4	716.4
DR44	4279	183.6	1212
DR45	4157	163	1074
DR47	4173	144	947.1
DR48	4170	148	973.8
XZDR9	5030	185.4	1223
XZDR11	4377	102	667
XZDR15	4733	236	1561
CKLSQ	4839	216.5	1431

Quaternary graben of the Xurucuo-Chazi area. The Xurucuo-Chazi area is composed of a stepped normal fault in the NW direction and cuts the early NWW direction into various structural units. The Quaternary, the NW-trending fault zone, has been active for many times, thus controlling the evolution of graben basins. Basin margin faults form linear fault triangles. The NNE, NNW, and SN directions are connected end to end, showing the characteristics of tracking faults. A series of hot springs or cold water springs are linearly distributed along the active faults on both the sides of the graben. The SN-trending graben was formed in the area because the collision of the Paleogene Indian plate with the Gangdise plate, and the Indian plate continued to push northward, thus forming an intra-continental orogenic uplift on both the sides of the fault basin. The crust uplifts to a certain height, forming two sets of rupture surfaces in NE and NW directions. The uplifted high mountains form fault-block mountains (uplift belts), resulting in an altitude of 6000 m on both the sides of the fault depression, such as the Duo Zebu Mountain. The neotectonic belts in the study area are mostly closely associated with uplifts and fault depressions. Numerous fault depression zones often constitute several bead-shaped fault basins and lakes. These fault basins are often suitable places for hydrothermal activities. For example, the grid framework active structural belt and the Xu Rucuo active structural belt constitute several bead-shaped fault basins, boundary faults, and uplift mountain bodies. Combined with the great contribution of the local melt in the shell to the heat source, that is, the heat source background in the high-temperature geothermal display area of southern Tibet, the author suggests that the good heat source conditions in this study area are created under the complementary effects of local melts, tectonic movement, hydrothermal activity, and seismic activity.

5.2. *Migration Channel of Underground Hot Water in the Study Area.* Structural fractures are often favourable places for underground hot water storage and migration. The hydrothermal activity in the study area is mainly controlled by the Dajeling-Angren-Renbu-Langxian-Metuo fault, which extends in the EW direction in the northern boundary of the Yarlung Zangbo River junction and the Dangre Yongcuo-Xu Rucuo fracture that spreads in the SN direction. In the study area, Semi Hot Springs, Chazi Hot Springs, and other high-temperature hydrothermal display areas are exposed in the fault basin controlled by these faults. The Chazi fault and Duozebu fault spread in the near SN direction, the Zharinanmu Co South-Cuomei fault spreads in the near EW direction, and other secondary faults intersect with the main fault in the northwest and northeast directions. A huge underground water transport network is formed, which provides good conditions for the upwelling and transport of underground hot water from the deep.

5.3. *Thermal Storage Analysis.* The reservoirs in the study area are divided into shallow and deep reservoirs. The shallow thermal storage is chiefly Quaternary loose rock pore water-bearing rock group, and the lithology is alluvial-diluvial sandy gravel layer. The deep thermal storage is mainly bedrock fractured water-bearing rock group and mainly constitutes magmatic rocks with well-developed fractures and high permeability [60]. The fractures in the rock mass are developed, and the main faults are the intersection fracture zones. These fault fracture zones are underground hot water reservoirs.

The cap rocks in the study area chiefly constitute the rock masses of the Pana and Dianzhong Formations. The lithology is mainly shale, sandstone, limestone, andesite, etc. They have low thermal conductivity, large thickness, high water resistance, and heat retention, providing suitable heat retention conditions for the underground hot water in the study area.

Based on the aforementioned analysis, conclusions, and previous research results, the conceptual model of geothermal origin for the study area is summarised. The geothermal fluid in the study area mainly receives the infiltration and replenishment of atmospheric precipitation and snowmelt water, and the replenishment area is roughly located in the Duozebu mountainous area from the southwest. The cold water forms the infiltration of faults along the strong tectonic activity. As the distance from the deep magma melt gets closer, the temperature gradually increases. When the appropriate conditions are reached, it migrates upwards and continuously dissolves with the surrounding rock during migration. It exists in magmatic rocks with well-developed fissures and high permeability, forming deep thermal reservoirs. Because the bedrock fissure thermal reservoir is not completely enclosed, the underground hot water continues to migrate upward along the basement fissure and enters the Quaternary aquifer, creating a shallow thermal reservoir. Near the surface, the geothermal fluid is mixed with the cold water on the surface and is exposed at the topographical cut to form hot springs (Figure 10).

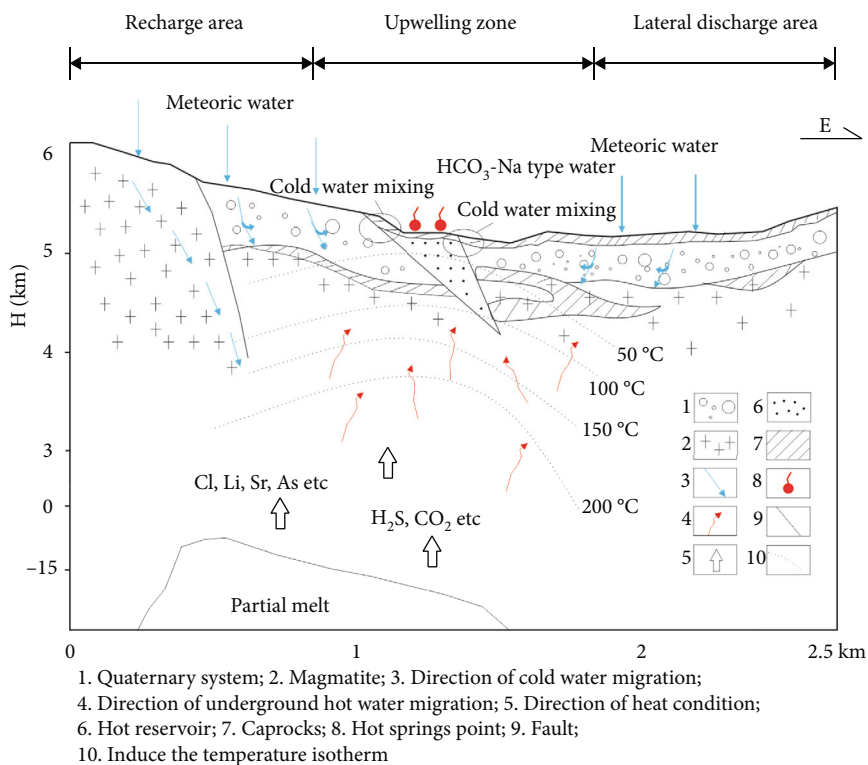


FIGURE 10: Concept model of the geothermal origin in the study area.

## 6. Conclusions

- (1) The geothermal area of Chazi, Tibet, features high-temperature geothermal reservoirs, and its hot water is moderately alkaline with high salinity and the hydrochemical type of  $\text{HCO}_3\text{-Na}$ . The ratio of  $\text{Na}^+/\text{Cl}^-$  is considerably  $>1$ , indicating that the groundwater undergoes dramatic dissolution that enables  $\text{Na}^+$ ,  $\text{K}^+$ , and  $\text{Ca}^{2+}$  available in potash feldspar and plagioclase to migrate into hot water. The  $\text{HCO}_3^-$  content in the geothermal water is considerably higher than that in the river water, which might indicate the dilution of hot water where runoff occurs after upwelling with the mixed surface cold water, enriching cold water with  $\text{HCO}_3^-$ .
- (2) The  $\delta^2\text{H}$ - $\delta^{18}\text{O}$  isotope analysis revealed that the main recharge source in the Chazi geothermal area is atmospheric precipitation, with no obvious  $\delta^{18}\text{O}$  drift. According to the height effect of  $\delta^2\text{H}$  and  $\delta^{18}\text{O}$  on precipitation, the recharge elevation is 5200–6000 m.
- (3) The temperature of geothermal reservoirs was estimated and corrected using geochemical thermometers, silica enthalpy, and the mixture model of chlorine enthalpy. The temperature of geothermal reservoirs in shallow areas is 143.7–150.6°C, and that in deep areas is 200~233°C; the average mixing ratio of cold water is 75%, and the average circulation depth is 1163 m.
- (4) The comprehensive analysis indicated that deep hot water mixes with cold water during upwelling and reaches the deep thermal reservoir layer. Subsequently, the mixed water rises, again mixing with shallow cold water and reaching the shallow thermal reservoir layer. The NW normal fault provides a channel for deep geothermal excretion, and the sand gravel layer of the quaternary alluvium creates a cover for thermal reservoirs. The prominent recharge direction is from alpine to valley, and the main source of recharge is ice and snow meltwater, followed by atmospheric precipitation.

## Data Availability

The data used to support the findings of this study are available from the corresponding author upon request.

## Conflicts of Interest

There is no conflicts of interest regarding the publication of this paper.

## Acknowledgments

This research was funded by the project the National Natural Science Foundation of China (Grant no. U1906209, 42072331, 41877192, and 41502220), Shandong Province Key R&D Program Funded Project (Grant no. 2019GSF109053), the National Science Foundation of Tibet

Autonomous Region (Grant no. XZ2019ZRG-158 and XZ202001ZR0044G), and the central government guides local projects (Grant no. XZ202201YD0029C).

## References

- [1] Z. Yanping, L. Min, H. Yu, W. Hongbin, and C. Duofu, "Corrigendum to "an areal assessment of subseafloor carbon cycling in cold seeps and hydrate-bearing areas in the northern South China Sea"," *Geofluids*, vol. 2019, Article ID 5107250, 1 pages, 2019.
- [2] D. Ji, "Geothermal resources and utilization in Tibet and the Himalayas," in *Workshop for decision makers on direct heating use of geothermal resources in Asia*, pp. 11–18, Tianjin, China, 2008.
- [3] X. Ma, S. Attia, T. Cawood, W. Cao, Z. Xu, and H. Li, "Arc tempos of the Gangdese batholith, southern Tibet," *Journal of Geodynamics*, vol. 149, 2022.
- [4] Z. Ping, J. Jin, Z. Haizheng, D. Ji, and L. Tingli, "Chemical composition of thermal water in the Yangbajing geothermal field, Tibet," *Chinese Journal of Geology*, vol. 33, no. 1, pp. 61–72, 1998.
- [5] P. Zhao, M. Kennedy, J. Dor et al., "Noble gases constraints on the origin and evolution of geothermal fluids from the Yangbajing geothermal field, Tibet," *Acta Petrologica Sinica*, vol. 17, no. 3, pp. 497–503, 2001.
- [6] D. Ji, "The basic characteristics of the Yangbajing geothermal field—a typical high temperature geothermal system," *Engineering Science*, vol. 5, no. 1, pp. 42–47, 2003.
- [7] G. Qinghai and Y. Chen, "Tungsten anomaly of the high-temperature hot springs in the Daggyai hydrothermal area, Tibet, China," *Earth Science*, vol. 46, no. 7, pp. 2545–2553, 2021.
- [8] L. Shijuan, *The Provenance Analysis of the Medium-High Temperature Geothermal Fluid in Cona, Tibet*, Hebei GEO University, 2016.
- [9] G. Qinghai, W. Yanxin, and L. Wei, "Hydrogeochemistry and environmental impact of geothermal waters from Yangyi of Tibet, China," *Journal of Volcanology and Geothermal Research*, vol. 180, no. 1, pp. 9–20, 2009.
- [10] W. Kunyu, S. Licheng, W. Xianggui, X. Qiong, and W. Peng, "Study on hydrochemical features of hot springs in Langjiu geothermal field, Tibet, China," *Carsologica Sinica*, vol. 30, no. 1, pp. 1–7, 2011.
- [11] L. Zhao, C. Kang, and N. Dawa, "Hydrochemical characteristics of geothermal water in Gudui, Xizang(Tibet)," *Geological Review*, vol. 63, pp. 353–354, 2017.
- [12] Z. Yunhui, *Research on Genesis and Development of the Geothermal System in the Kangding-Moxi Segment of the Xianshuihe Fault*, Chendu University of technology, 2018.
- [13] W. Sien, "The Xigaze group and its significance in plate tectonic," *Professional Papres of Stratigraphy and Palaeontology*, vol. 2, pp. 133–140, 1988.
- [14] L. Baojun, Y. Guangming, and C. Chengsheng, "Ophiolitic submarine fans and their Plate tectonic settings in the Xigaze group along the Yarlung Zangbo suture zone in Xizang," *Sedimentary Facies and Palaeogeography*, vol. 13, no. 2, pp. 13–24, 1993.
- [15] F. Yangang, T. Juxing, H. Guyue, G. Yiming, and L. Bin, "The magma records and mineralization of early subduction of Neo-Tethyan oceanic slab: zircon U-Pb and Hf isotopic composition of granitoids in the northwest of Xigaza," *Geological Bulletin of China*, vol. 37, no. 6, pp. 1026–1036, 2018.
- [16] F. Derong, L. Xun, and Y. Peiyi, "The late Jurassic-cretaceous sedimentary-tectonic development of the southern Xizang," *Bulletin of the Chinese Academy of Geological Science*, vol. 2, pp. 21–40, 1990.
- [17] H. Jie and L. Rijun, "Tectonic and sedimentary evolution of the Xigaze remnant-type forearc basin," *Journal of Graduate School, Academia Sinica*, vol. 14, no. 1, pp. 51–56, 1997.
- [18] J. Hao, Y. C. Chai, and J. L. Li, "Original tectonic setting of the Tsangpo ophiolite and sedimentary evolution of the Xigaze forearc basin," *Chinese Journal of Geology*, vol. 34, no. 1, pp. 1–9, 1999.
- [19] C. Jianlin, X. Jifeng, K. Zhiqiang, and W. Baodi, "Geochemistry and origin of Miocene volcanic rocks in Cazé area, southwestern Qinghai-Xizang plateau," *Geochimica*, vol. 36, no. 5, pp. 437–447, 2007.
- [20] N. Xiaolu, Z. Zhidan, M. Xuanxue et al., "Elemental and Sr-Nd-Pb isotopic geochemistry for basic rocks from Decun-Angren ophiolites in Xigaze area, Tibet: implications for the characteristics of the Tethyan upper mantle domain," *Acta Petrologica Sinica*, vol. 22, no. 12, pp. 2875–2888, 2006.
- [21] Y. Xiaodong, "Elementary analysis on the features and prevention measures of geological hazards in the Lhasa-Xigaze railway," *Gansu Science and Technology*, vol. 26, no. 10, pp. 28–29, 2010.
- [22] J. Jianfu, *Study on Geological Hazard Susceptibility Evaluation based on GIS of Shigatse*, Jilin University, 2015.
- [23] M. L. Ran, Z. Q. Kang, J. F. Xu et al., "Geochronology, geochemistry and geological significance of the Bima formation volcanic rocks located on the southern margin of the Lhasa block, Xigaze, Tibet," *Geochimica*, vol. 46, no. 3, pp. 205–218, 2017.
- [24] L. Yong, Z. Shizhen, L. Fengqi, Q. Yadong, and G. Xiaodong, "Zircon U-Pb ages and implications of the Dianzhong formation in Chazi area, middle Lhasa block, Tibet," *Earth Science*, vol. 43, no. 8, pp. 2755–2766, 2018.
- [25] P. Guixiong, "Experimental study on dressing process circuits of Zhazi Pb-Zn deposit in Tibet," *Gansu Metallurgy*, vol. 4, pp. 36–37, 2007.
- [26] Z. Yongsheng, F. Xiaowei, Y. Erjun, and W. Zhixiong, "The geological and geochemical characteristics and prospecting criteria of Ngamring county Chazi lead-zinc polymetallic deposit in Tibet," *China Mining Magazine*, vol. 22, no. S1, pp. 143–148, 2013.
- [27] L. Haoting, G. Ning, S. Huixiao, L. Zhao, and N. Dawa, "Analysis of hydrochemical characteristics of the Chazi thermal spring in Tibet," *Geological Review*, vol. 65, no. S1, pp. 3–4, 2019.
- [28] L. Shaoqiang, X. Lin, T. Hua, X. Jin, and H. Lin, "Hydrochemical and isotopic characteristics of Chazi geothermal field in Shigatse in Tibet," *Geological Survey of China*, vol. 7, no. 5, pp. 10–15, 2020.
- [29] T. Wei, L. Zhijie, L. Shibin, Z. Zhifei, M. You, and Z. Mingtao, *Thermal Springs in Tibet*, Science Press, Beijing, 2000.
- [30] S. Mwangi, "Application of geochemical methods in geothermal exploration in Kenya," *Procedia Earth and Planetary Science*, vol. 7, pp. 602–606, 2013.
- [31] Z. Shizhen, L. Yong, L. Fenqi, Q. Yadong, and G. Xiaodong, "Zircon U-Pb geochronology, geochemistry and petrogenesis

- of the Miocene syenite in Chazi area, Tibet,” *Earth Science*, vol. 45, no. 8, pp. 2882–2893, 2020.
- [32] L. Shaoqiang, N. Dawa, L. Huan, C. Fujun, G. Sangpingcuo, and L. Songqunpei, “Geological structure characteristics and genetic mechanism of the Caze geothermal field in Xikaze, Tibet,” *Acta Geologica Sichuan*, vol. 40, no. 1, pp. 30–33, 2020.
- [33] Y. Haoran, *Discussion on Metallogenic Potential of Chazi Area in Tibet*, Chendu University of technology, 2019.
- [34] M. L. Li, J. Duo, Z. Wang, G. D. Wu, Z. Z. Jiang, and G. L. Liu, “Hydrochemical characteristics and material sources of the Riduo, thermal spring in Tibet,” *Carsologica Sinica*, vol. 34, no. 3, pp. 209–216, 2015.
- [35] L. Haoting, *Chemical Characteristics and Provenance Analysis of Geothermal Water in a Typical Geothermal Display Area in Angren County, Tibet*, Hebei GEO University, 2020.
- [36] H. Sun, F. Ma, Z. Liu, Z. Liu, G. Wang, and D. Nan, “The distribution and enrichment characteristics of fluoride in geothermal active area in Tibet,” *China Environmental Science*, vol. 35, no. 1, pp. 251–259, 2015.
- [37] Y. Palabiyik and U. Serpen, “Geochemical assessment of Simav geothermal field, Turkey,” *Revista Mexicana de Ciencias Geológicas*, vol. 25, no. 3, pp. 408–425, 2008.
- [38] M. Redwan, A. A. Abdel Moneim, and M. A. Amra, “Effect of water–rock interaction processes on the hydrogeochemistry of groundwater west of Sohag area, Egypt,” *Arabian Journal of Geosciences*, vol. 9, no. 2, 2016.
- [39] Y. A. Kettanah and A. H. Bamarni, “Petrogenesis, geochemistry, and tectonic setting of a basaltic body within the Gercus formation of northern Iraq: first record for Eocene anorogenic volcanic activity in the region,” *Turkish Journal of Earth Sciences*, vol. 6, pp. 460–491, 2018.
- [40] M. Afsin, D. M. Allen, D. Kirste, U. G. Durukan, A. Gurel, and O. Oruc, “Mixing processes in hydrothermal spring systems and implications for interpreting geochemical data: a case study in the Cappadocia region of Turkey,” *Hydrogeology Journal*, vol. 22, no. 1, pp. 7–23, 2014.
- [41] L. Gongke, W. Weixing, Y. Fengtiao, L. Hong, S. Jian, and D. Luyang, “Genesis model of the Tangquan geothermal field in Hebei Province,” *Geoscience*, vol. 29, no. 1, pp. 220–228, 2015.
- [42] Z. Meng, L. Wenjing, L. Zhao, L. Zhiming, H. Xiancai, and W. Guiling, “Hydrogeochemical characteristics and genetic model of Gulu high-temperature geothermal system in Tibet, China,” *Journal of Chengdu University of Technology (Science & Technology Edition)*, vol. 41, no. 3, pp. 382–392, 2014.
- [43] G. Sergio, A. Michele, P. Maddalena, and C. Gianni, “Identifying sources of B and as contamination in surface water and groundwater downstream of the Larderello geothermal–industrial area (Tuscany–Central Italy),” *Journal of Hydrology*, vol. 509, pp. 66–82, 2014.
- [44] E. Kalacheva, Y. Taran, T. Kotenko, K. Hattori, L. Kotenko, and G. Solis-Pichardo, “Volcano–hydrothermal system of Ebeko volcano, Paramushir, Kuril Islands: geochemistry and solute fluxes of magmatic chlorine and sulfur,” *Journal of Volcanology and Geothermal Research*, vol. 310, pp. 118–131, 2016.
- [45] S. P. Verma, “Origin, evolution, and tectonic setting of the eastern part of the Mexican Volcanic Belt and comparison with the central American volcanic arc from conventional multielement normalized and new multidimensional discrimination diagrams and discordancy and significance tests,” *Turkish Journal of Earth Sciences*, vol. 2, pp. 111–164, 2015.
- [46] F. Bégué, C. D. Deering, D. M. Gravley, I. Chambefort, and B. M. Kennedy, “From source to surface: Tracking magmatic boron and chlorine input into the geothermal systems of the Taupo Volcanic Zone, New Zealand,” *Journal of Volcanology and Geothermal Research*, vol. 346, pp. 141–150, 2017.
- [47] T. Wei, Z. Mingtao, Z. Zhifei et al., *Geothermals Beneath Xizang(Tibetan)*, Science Press, Plateau, 1981.
- [48] D. Oyuntsetseg, D. Ganchimeg, A. Minjigmaa, A. Ueda, and M. Kusakabe, “Isotopic and chemical studies of hot and cold springs in western part of Khangai Mountain region, Mongolia, for geothermal exploration,” *Geothermics*, vol. 53, pp. 488–497, 2015.
- [49] R. M. Shoedarto, Y. Tada, K. Kashiwaya, K. Koike, and I. Iskandar, “Specifying recharge zones and mechanisms of the transitional geothermal field through hydrogen and oxygen isotope analyses with consideration of water–rock interaction,” *Geothermics*, vol. 86, article 101797, 2020.
- [50] J. J. T. Dimabayao, M. C. Rowe, and S. Barker, “Stable isotope systematics of fluids and epidote in the bacon-Manito geothermal field, Philippines: indicators of fluid origin and evolution,” *Geothermics*, vol. 80, pp. 31–43, 2019.
- [51] H. Craig, “Isotopic variations in meteoric waters,” *Science*, vol. 133, no. 3465, pp. 1702–1703, 1961.
- [52] A. Rufai, N. Moshood, and D. S. Tijani, “Hydrochemistry and stable isotopes ( $^{18}\text{O}$  and  $^2\text{H}$ ) characteristics of groundwater in Lokoja and its environs, central Nigeria,” *Environmental Earth Sciences*, vol. 78, no. 19, 2019.
- [53] M. O. Awaleh, T. Boschetti, A. E. Adaneh et al., “Hydrochemistry and multi-isotope study of the waters from Hanlé-Gaggadé grabens (Republic of Djibouti, East African Rift System): a low-enthalpy geothermal resource from a transboundary aquifer,” *Geothermics*, vol. 86, article 101805, 2020.
- [54] Y. Jinsheng, Z. Hongbin, Y. Fuji, and L. Deping, “Oxygen isotopic composition of meteoric water in the eastern part of Xizang,” *Geochimica*, vol. 2, pp. 113–121, 1980.
- [55] R. O. Fournier, “Chemical geothermometers and mixing models for geothermal systems,” *Geothermics*, vol. 5, no. 1–4, pp. 41–50, 1977.
- [56] W. F. Giggenbach, “Geothermal solute equilibria. Derivation of Na–K–Mg–Ca ge indicators,” *Geochimica et Cosmochimica Acta*, vol. 52, no. 12, pp. 2749–2765, 1988.
- [57] P. M. K. Das and D. Padmalal, “Hydrochemistry, geothermometry and origin of the low temperature thermal springs of South Konkan region, India,” *Geothermics*, vol. 90, article 101997, 2021.
- [58] P. Zhao, M. Kennedy, J. Dor et al., “Noble gases constraints on the origin and evolution of geothermal fluids from the Yangbajain geothermal field, Tibet,” *Acta Petrologica Sinica*, vol. 17, no. 3, pp. 497–503, 2001.
- [59] Z. Ciping, R. Hua, and C. Kunhua, “Present-day magma chambers in Tengchong volcano area inferred from relative geothermal gradient,” *Acta Petrologica Sinica*, vol. 22, no. 6, pp. 1517–1528, 2006.
- [60] Z. Li, *Characteristics of the typical hot springs in the Central Tibet*, China University of Geosciences(Beijing), 2012.